2011 American Control Conference
on O'Farrell Street, San Francisco, CA, USA
June 29 - July 01, 2011

A Model Based Feedback Controller for Wing-Twist via Piezoceramic Actuation

Cody W. Ray and Belinda A. Batten
School of Mechanical, Industrial,
& Manufacturing Engineering
Oregon State University
Corvallis, OR
Email: raycod@onid.orst.edu
bbatten@engr.orst.edu

John R. Singler
Department of Mathematics & Statistics
Missouri University of Science & Technology
Rolla, Missouri 65409-0020
Email: singlerj@mst.edu

Abstract— **In this paper we present a model for a rubber plate with piezoceramic actuators to represent a bioinspired flexible wing. Using a Galerkin based finite element approximation to the system, we compute a linear quadratic based tracking control for piezoelectric actuators placed along both leading and trailing edges. Using these piezoceramic devices, we demonstrate the effectiveness of model based feedback control in achieving a desired wing tip position; this modified shape is analogous to aircraft roll moment generation via wing twist.**

I. Introduction

One recent area of research in micro air vehicle (MAV) control is concerned with morphing wing structures rather than using traditional control surfaces for maneuvers. Morphing for flight control was first utilized on the Wright Flyer in 1903. Cables were attached in a way to allow the pilot to twist the wings to achieve a desired configuration. Due to power requirements of actuators to change the shape of the wings, wing morphing methods were largely abandoned [1]. Recently, flexible and morphing wing research and technology has renewed interest, and promises to greatly enhance performance of aircraft [2], [3]. A continuous morphing design can achieve a greater variety of desired wing shapes and more precise camber control while simultaneously reducing friction and discontinuities introduced by traditional actuators such as rudders and flaps. For instance, A rigid wing design experiences performance drops for low Reynolds number regimes ($Re < 10^5$), whereas a flexible wing benefits overall aerodynamic performance through mechanisms such as passive shaping [4], [5]. Many recent studies indicate that a variety of performance gains can be made by allowing an airfoil to deform in flight, see for example, [6]–[9]. Munday and Jacoby [10], among others, demonstrated that separation could be reduced significantly by oscillating the camber of an airfoil, as compared to a static wing at the same angle of attack.

Standard aircraft control surfaces achieve sufficient control authority for flight of larger aircraft, but have substantially reduced effectiveness for MAVs. Wing morphing has the potential to enhance MAV performance by adapting the wing shape to specific environments [2] and increase maneuverability by using continuous wing shape change rather than standard discrete control surfaces [11]. Although many morphing designs have been proposed, very few have been tested in MAVs [12].

Abdulrahim et al. [12] and Stanford et al. [13] directly applied a few very basic wing morphing techniques and demonstrated that a wing made out of a flexible material can be morphed with little power, but with great benefit to performance. Interestingly, these morphing and camber control methods are all actuation schemes available to biological flyers [14]–[16]. Achieving morphing and camber control in a continuous, unobtrusive goal of incorporating smart materials into flexible MAV designs [17]. It has been shown that hubs, hinges, and cables create discontinuities over the wing surface which can lead to airflow separation [18].

Bae et al. [19] demonstrated camber control of a flexible wing using piezoelectric actuation. However, their study, like most that deal with piezoelectric control, was limited to larger unmanned air vehicles. Very little work has been done on wing morphing with smart materials, at least at the 15-30 cm wingspan scale, which is the topic of this work.

Our long range goal is to construct a closed loop system of a membrane wing with smart actuators and hair cell sensors studied extensively by Dickinson [20]–[22] to sense flow over the wing. The overall aerodynamic properties under a variety of flow conditions would be studied, particularly how camber changes affect flight performance. In this paper, we present a cantilevered thin plate with piezoceramic actuators strategically placed along the spanwise direction such that plate (wing) tip twist is possible by activating the actuators out of phase. We then consider the closed loop tracking performance of the system in response to prescribed initial conditions and external forcing. Specifically, the work entails achieving a desired state like that shown in figure (1(b)), which is very similar to the twisting wing MAV of [12], [13]. It is our hypothesis that achieving wing tip twist using smart materials will allow for greater control over aerodynamic maneuvers and is also a needed investigation into utilizing smart materials as aerodynamic loading sensors

978-1-4577-0079-8/11/$26.00 ©2011 AACC

and estimators.

A. Model Derivation

The inspiration for our investigations comes from a bat's ability to change the camber of and morph its wing through muscles embedded in the skin. Specifically, the bat wing is composed of an anisotropic membrane surface (skin) stretched over a network of bones with muscles to control flapping and maintain tension during flight (see Figure 1a). We begin our work with a model of a wing segment constructed of a cantilevered thin plate surrounded by a thin sections of a material of greater modulus of elasticity on the edges, excluding the free (wing tip) edge. This model assumes the stiffer edge frame supports the more flexible inner domain under prestrain, such that linear elasticity theory applies.

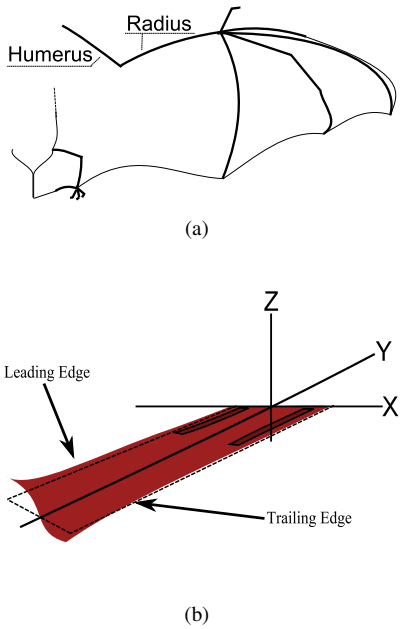

Fig. 1. (a) Bat wing schematic and (b) twisting cantilevered plate system with two piezoceramic actuators

The bat wing membrane is highly anisotropic and varies up to 1000:1 in spanwise vs chordwise stiffness [23]. The system used in this work was chosen to be orthotropic, with stiffness less in the chordwise and greater in the spanwise direction (see table I). Material parameters were chosen to that the interior of the plate is a rubber-like pre-strained material undergoing small deflections and the beam support is aluminum. This allows for large spanwise edge deflection while still satisfying thin plate model criteria.

Detailed derivations of of the model of an orthotropic plate can be found in a variety of textbooks on thin plate theory such as [24]. Following standard stress analysis methodology, balancing moment and shear forces, we obtain the standard orthotropic plate model, where it is assumed that one sums the contributions of all the piezoceramic patches. Here we have written the equation to include the contribution from

TABLE I
MATERIAL PARAMETERS

	Plate/Beam	Patch
$L(m)$	.60	.3
$W(m)$	.15	.0375
$h(m)$	.0005/.005	.003
$E_x(GPa)$	.1	28.6
$E_y(GPa)$	1.0/69	28.6
ν_x, ν_y	.3	.3
$C_D(N\,m\,s)$	$1.4e{-4}$	$1.4e{-4}$
$\rho(kg/m^3)$	1000	5300
$d_{31}(m/v)$	n/a	$290e{-12}$

the ith patch using formulae from [25].

$$\rho h w_{tt} - (M_x)_{xx} - (M_y)_{yy} - (M_{xy})_{yx} - (M_{yx})_{xy} = \hat{f}_n(t) + \left[((M_y)_{pz})_{yy} + ((M_x)_{pz})_{xx}\right]_i, \quad (1)$$

where

$$M_x = D_x\left(-w_{xx} - \nu_y w_{yy}\right) + C\left(-w_{txx} - \nu_y w_{tyy}\right) + \left[D_{pz}\left(-w_{xx} - \nu_y w_{yy}\right) + C_{pz}\left(-w_{txx} - \nu_y w_{tyy}\right)\right]\chi_i(x,y)$$
$$M_y = D_y\left(-w_{yy} - \nu_x w_{xx}\right) + C\left(-w_{tyy} - \nu_x w_{txx}\right) + \left[D_{pz}\left(-w_{yy} - \nu_x w_{xx}\right) + C_{pz}\left(-w_{tyy} - \nu_y w_{txx}\right)\right]\chi_i(x,y)$$

$$M_{xy} = G\left[-2w_{yx}\right] + G_{pz}\left[-2w_{tyx}\right] + C_G\left[-2w_{yx}\right] + C_{Gpz}\left[-2w_{tyx}\right]\chi_i(x,y)$$
$$M_{yx} = G\left[-2w_{yx}\right] + G_{pz}\left[-2w_{tyx}\right] + C_G\left[-2w_{yx}\right] + C_{Gpz}\left[-2w_{tyx}\right]\chi_i(x,y)$$
$$(M_y)_{pz} = \frac{E_{pz} d_{31}}{4h_{pz}(1-\nu_{pz})}\left(4\left(\frac{h}{2}+h_{pz}\right)^2 - h^2\right)V_i(t)$$
$$(M_x)_{pz} = \frac{E_{pz} d_{31}}{4h_{pz}(1-\nu_{pz})}\left(4\left(\frac{h}{2}+h_{pz}\right)^2 - h^2\right)V_i(t),$$

$$D_x = \frac{E_x\, h^3}{12(1-\nu_x\nu_y)} \qquad D_{pz} = \frac{2E_{pz}\, a_3}{3(1-\nu_{pz}^2)}$$

$$D_y = \frac{E_y\, h^3}{12(1-\nu_x\nu_y)}$$

$$G = \frac{E_x h^3}{24(1+\nu_x)} \qquad G_{pz} = \frac{E_{pz} a_3}{3(1+\nu_{pz})}$$

$$C = \frac{c_D\, h^3}{12(1-\nu_x\nu_y)} \qquad C_{pz} = \frac{2c_{Dpz}\, a_3}{3(1-\nu_{pz}^2)}$$

$$C_G = \frac{c_D h^3}{24(1+\nu_x)} \qquad C_{Gpz} = \frac{c_{Dpz} a_3}{3(1+\nu_{pz})},$$

and

$$\chi_i(x,y) = \begin{cases} 1 & x_1 \le x \le x_2\,,\, y_1 \le y \le y_2 \\ 0 & \text{otherwise} \end{cases} \quad (2)$$

represents a step function describing the position of the piezoceramic on the plate.

Multiplying equation (1) by test functions $\phi(x)$ and integrating by parts (or applying the divergence theorem in component form, found in [26]) we arrive at the weak form of the plate equation. After application of relevant boundary conditions we arrive at

$$\int_{\Omega} \left[((\rho_p h w_{tt} - \hat{f}_n(t))\phi - (M_x)\,\phi_{xx} - (M_y)\,\phi_{yy} - (M_{xy})\,\phi_{yx} - (M_{yx})\,\phi_{xy} + \left[((M_y)_{pz})\,\phi_{yy} + ((M_x)_{pz})\,\phi_{xx}\right]_i\right] d\Omega = 0. \quad (3)$$

II. Finite Element Approximation

To form the Galerkin finite element approximation for this system, we make the substitution,

$$w(t,x,y) \approx \sum_{i=1}^{N} z_i(t)\,\phi_i\,(x,y),$$

into the weak form equation of the system (3). We choose the shape functions ϕ to be bicubic B-splines on a rectangular mesh. Substituting these terms into equation (3) and simplifying yields

$$M\ddot{z} + C\dot{z} + Kz = \hat{B}u(t) + \hat{F}(t),$$

where dots are used to indicate differentiation in time. This is the finite element matrix approximation to the plate system PDE. For a detailed derivation to a similar model, see [27].

For simulation and control purposes, we write this system in first order state space form with initial condition as

$$\dot{z} = Az + Bu(t) + F(t), z(0) = z_0 \quad (4)$$

where

$$A = \begin{bmatrix} 0 & I \\ -M^{-1}K & -M^{-1}D \end{bmatrix} \quad (5)$$

$$B = \begin{bmatrix} 0 \\ M^{-1}\hat{B} \end{bmatrix}, \qquad F = \begin{bmatrix} 0 \\ M^{-1}\hat{F} \end{bmatrix}. \quad (6)$$

III. Control Methodology

We begin with the model in equations (4) - (6)

$$\dot{z} = Az + Bu(t) + F(t), z(0) = z_0.$$

Making the substitution $x = z - z_d$, where z_d is the desired function to track, we obtain

$$\begin{aligned} \dot{x} &= Ax + Bu(t) + F(t) + (Az_d - \dot{z}_d), \\ x(0) &= z(0) - z_d(0). \end{aligned}$$

Since the matrix A, the functions z_d, and $\dot{z}_d$ are known, the problem then becomes one of driving the tracking error x to zero. Thus the problem statement is summarized as: given the known disturbance $d(t)$, find the control $u^*(t)$ such that $u^* = \min_u J(u)$, where

$$J = \int_0^{t_f} x^T Q x + u^T R u,$$

subject to the constraints

$$\begin{aligned} \dot{x} &= Ax + Bu + F(t) + d \\ d &= Az_d - \dot{z}_d \\ x(0) &= z(0) - z_d(0). \end{aligned}$$

The Differential Ricatti Equation (DRE), and a matrix equation for feed forward signal b must be solved to obtain the optimal control law $u(t)$,

$$-\dot{\Pi} = \Pi A + A^T\Pi - \Pi B R^{-1} B^T \Pi + Q \quad (7)$$

$$b = \left(A - BR^{-1}B^T\Pi\right)^{-T} \Pi d, \quad (8)$$

Equation (7) is the general solution for $\Pi(t)$. Setting $\dot{\Pi} = 0$ yields the *steady state regulator* problem, in which the optimization time interval is infinite; this process yields the algebraic Ricatti equation (ARE),

$$0 = \bar{\Pi}A + A^T\bar{\Pi} - \bar{\Pi}BR^{-1}B^T\bar{\Pi} + Q,$$

where $\bar{\Pi}$ denotes the steady state solution for $\Pi(t)$. Thus the control problem for the finite element system is written

$$\begin{aligned} \dot{x}(t) &= Ax(t) + Bu(t) + F(t) + d(t) \\ d(t) &= Az_d(t) - \dot{z}_d(t) \\ u(t) &= -R^{-1}B^T\bar{\Pi}x(t) - R^{-1}B^T b(t), \end{aligned}$$

where $b(t)$ is the solution to equation (8).

IV. Numerical Results

For numerical experiments, two patches were assumed to be perfectly bonded to the beam support structures on the outer edges of the membrane. These patches extend from $x_1 = .15$m to $x_2 = .35$m along the beam as shown in Figure 1(b). A mesh consisting of N_x and N_y nodes in the x and y directions respectively, yields $2(N_xN_y + 2N_y)$ states in the system as a result of three free and one cantilevered edges. Three meshes were used in the numerical experiments to test convergence of the results, corresponding to $(N_x, N_y) = (9,33),(17,65),(33,129)$ nodes. In the following subsections, we show functional gains that define the control law and tracking simulations in the presence of external forcing. A discussion of functional gains can be found in [25], [27]–[29].

A. Control Gains and Convergence

In all computations, $R = 1e^{-5}$ was used. Control functional gains were calculated using the equation

$$[k_b\ k_v]^T = \begin{bmatrix} K & 0 \\ 0 & M \end{bmatrix}^{-1} K_c^T, \quad (9)$$

where k_b and k_v are the bending and velocity gains, respectively, and $K_c = R^{-1}B^T\bar{\Pi}$. To compute control functional

gains, the state weight Q was chosen to emphasize the tracking performance along the free edge ($y = 0$). Specifically,

$$Q = \begin{bmatrix} diag(q_i)K & 0 \\ 0 & M \end{bmatrix}, \tag{10}$$

with $q_i = 1e5$ for $i = 1, ...N_x$ and zero otherwise.

Convergence of the bending and velocity gains was verified for two patches along the spanwise plate edges as illustrated in Figures 2(a)-2(b). The patches were chosen to be one half of the plate length (30cm) and (3.75cm) in width such that they lie directly upon the finite element mesh nodes for the chosen mesh refinements. In figures 3(a)-4(b) the gains for the leading edge patch are plotted for grid resolutions 9×33 and 17×65 nodes corresponding to 8×32 and 16×64 square elements; the gains from the finest mesh did not differ significantly from those shown here. The gains for the trailing edge patch are perfectly symmetric with those for the leading edge shown here.

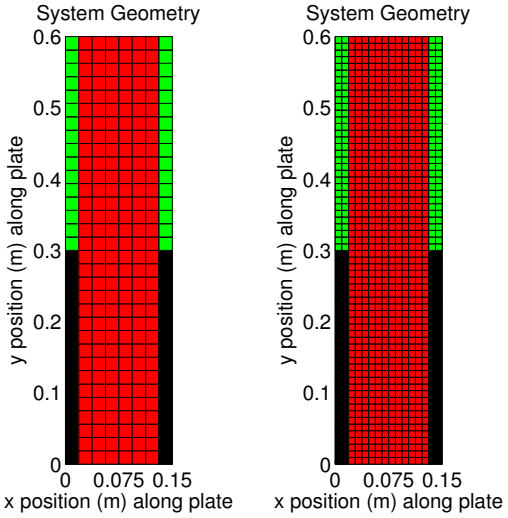

Fig. 2. (a) Geometry and mesh for node numbers $(N_x, N_y) = (9, 33)$ and (b) for $(N_x, N_y) = (33, 65)$ with plate in red, beam in black and piezoceramic actuators in green

Notice the location of the dominant features of the plots coincides with the location of the patch. As the number of elements gets larger, the surface plot features tend to the edge of the patch, becoming less two dimensional in support. Results such as these will be used to place sensors for the closed loop investigations of camber control, e.g. [28], [29].

B. Tracking with External Forcing

One set of simulations is presented here to demonstrate the control effectiveness of a piezoceramic in camber control. The simulations were obtained using the ODE23s stiff system Runge-Kutta integration routine in Matlab. Parameters used in this study are summarized in table I, and were held constant for all simulations. Patch parameters were taken from [30] and from online product parameter tables for highly deforming piezoceramic materials.

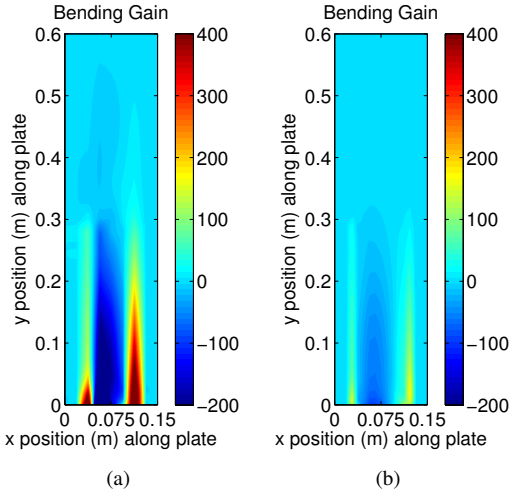

Fig. 3. (a) Bending gain for leading edge patch for $(N_x, N_y) = (9, 33)$ and (b) for $(N_x, N_y) = (33, 65)$

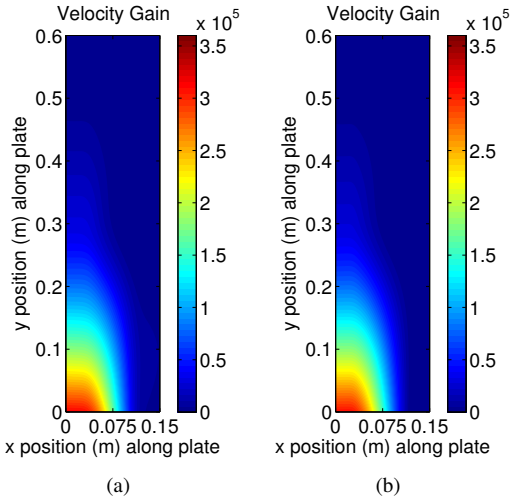

Fig. 4. (a) Velocity gain for leading edge patch for $(N_x, N_y) = (9, 33)$ and (b) for $(N_x, N_y) = (33, 65)$

To test the efficacy of a piezoceramic patch system on a plate to control wing twist in the presence of an external forcing function, we used the desired shape function as defined by the first mode shape of an Euler-Bernoulli beam, interpolated between the spanwise edges of the plate. Specifically, the desired position for the leading edge of the plate is the positive first mode of an Euler-Bernoulli beam, while the trailing edge is simply the same function with opposite sign. The full desired position for the plate is the linear interpolation of these two edges, thus the plate tip (wing tip) edge is linear but making an angle of approximately 7.5 degrees with the horizontal. Fully achieving the desired position for an overall aircraft angle of attack will in theory result in roll moments very similar to that described in [12], [13], and perhaps even greater so due to the continuous change in angle of attack in the spanwise direction.

The external forcing used in the simulation is given by

$$\hat{f}(t) = \frac{1}{2}(\frac{1}{2}\cos(25\pi t) + 4\cos(45\pi t) + .4\sin(15\pi t) + .. \\ 80\sin(90\pi t) - 60\cos(34\pi t) + .4 * \sin(17\pi t) + ... \\ \frac{1}{2}\cos(12\pi t) + \frac{1}{5}\sin(15\pi t) + 90\sin(61\pi t)).$$

This function is not meant to capture any realistic physics at this point, but rather to simply force the plate with both high and lower frequency components to illustrate the problem at hand. The force is not homogeneously distributed over the plate, rather it is distributed using a function similar to the desired state function, so that the maximum force occurs at the free corner and zero force occurs along the leading and clamped edges, with maximum force occurring at the free corner of the trailing edge.

In Figures 5(a)-6(c) we see the result of applying the aforementioned control methodology to this system. The plate is twisted into the desired position, thereby achieving a desired wing-top angle of attack (Figure 5(a)) as a result of the prescribed control illustrated in Figure 5(b). The external force is rejected except for the higher frequency components as illustrated in Figure 6(b).

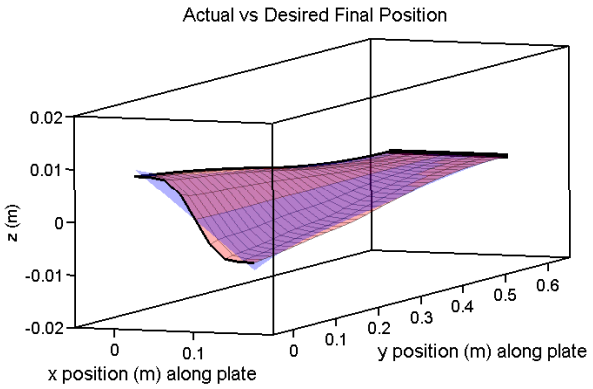

(a)

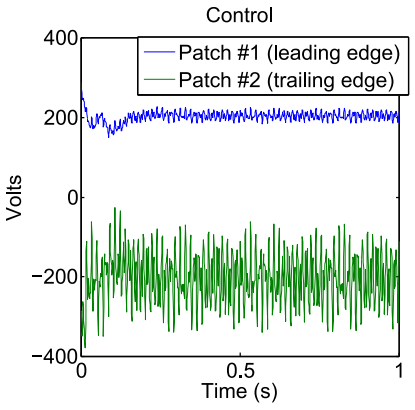

(b)

Fig. 5. (a) Final plate position (red) with desired (blue) and (b) control input

Note the voltage applied illustrated in Figure 5(b), the control required to maintain the desired position is at the

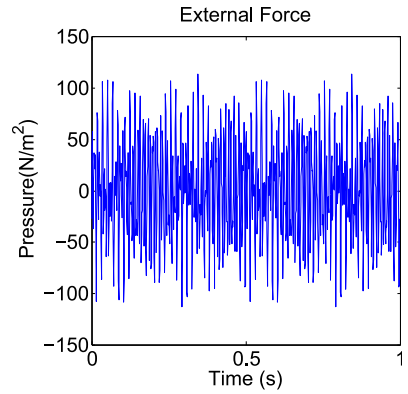

(a)

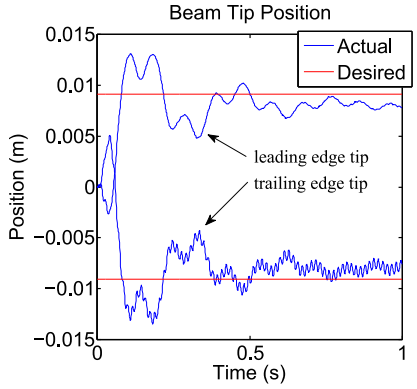

(b)

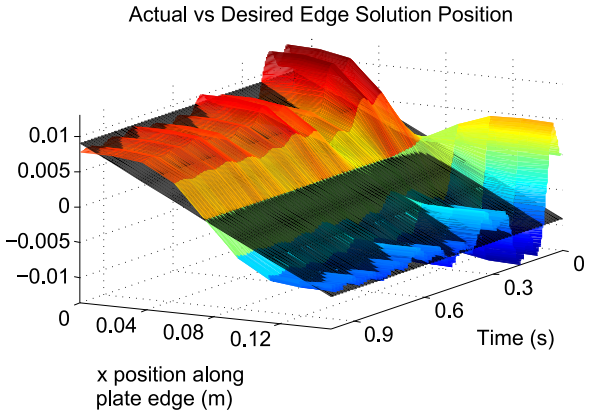

(c)

Fig. 6. (a) External pressure, (b) free corner positions for leading and trailing edges and (c) Plate edge position in time with desired position illustrated in black

realistic limit. While these results show that camber control of the overall system position with a piezoceramic is possible, further design research should be completed to bring required control effort to more realistic limits. Note also the shape of the free edge shape (appearing sinusoidal in shape in Figure 6(c)). It may be desirable to retain a linear shape for the free edge; how this may be achieved will be investigated in a later study.

V. Conclusion and Future Directions

In this work, we showed that piezoceramic patches along leading and trailing edges of a flexible rubber-like plate can

be used for steady state tracking control problems related to wing morphing and camber. We computed control functional gains corresponding to bending and velocity; results such as these can and will be used for sensor placement. We demonstrated a steady state tracking problem indicative of a wing maintaining a certain camber during flight. This problem was solved in the presence of an external periodic force. This work demonstrates that the aerodynamic consequences of this application of piezoceramics to flight systems has great potential, especially for aircraft in the $1m$ wingspan range.

There are drawbacks to using piezoceramics as actuators for MAVs, the most important of which is their very low control authority. Placement of more patches may alleviate this issue, as will the utilization of more flexible materials along with further investigation into optimal placement of actuators. The value of the control authority coefficient, R, could also be adjusted to maximize the potential of the piezoceramic device. Utilizing an experimental design rather than solely finite element simulation and theoretical parameters is an important next step in this research.

Immediate future work will include utilizing more patches in the domain to increase control authority, consider different types of smart material actuators, inclusion of sensors and an estimator design, and potentially a physically more meaningful external disturbance. This work will culminate with the use of real fluid flow simulation data, as well as the full fluid structure interaction problem.

ACKNOWLEDGMENT

This work was supported in part by the Air Force Office of Scientific Research under the Multidisciplinary University Research Initiative grant FA9550-07-1-0540.

REFERENCES

[1] B. Sanders, F. Eastep, and E. Forster, "Aerodynamic and aeroelastic characteristics of wings with conformal control surfaces for morphing aircraft," *Journal of Aircraft*, vol. 40, no. 1, pp. 94–99, 2003.

[2] J. Bowman, B. Sanders, and T. Weisshar, "Evaluating the impact of morphing technologies on aircraft performance," *AIAA*, vol. 2002-1631, 2002.

[3] A. DeLuca, "Experimental investigation into the aerodynamic performance of both rigid and flexible wing structured micro-air-vehicles," Master's thesis, Air Force Institute of Technology, Wright-Patterson Air Force Base, Ohio, 2004.

[4] W. Shyy, P. Ifju, and D. Viieru, "Membrane wing-based micro air vehicles," *ASME Transactions*, vol. 58, pp. 283–301, 2005.

[5] Y. Lian and W. Shyy, "Laminar-turbulent transition of a low reynolds number rigid or flexible airfoil," *AIAA Paper*, vol. 45, pp. 1501–1513, 2007.

[6] D. Jenkins, W. Shyy, J. Sloan, F. Klevebring, and M. Nilsson, "Airfoil performance at low reynolds numbers for micro air vehicle applications," in *Thirteenth Bristol International RPV/UAV Conference*. University of Bristol, 1998.

[7] R. Waszak, N. Jenkins, and P. Ifju, "Stability and control properties of an aeroelastic fixed wing micro air vehicle," *AIAA Paper*, vol. 2001-4005, 2001.

[8] R. Gordnier and M. Visbal, "Implicit les computations with applications to micro air vehicles," in *2009 DoD High Performance Computing Modernization Program Users Group Conference*, 2009.

[9] M. Visbal, R. Gordnier, and M. Galbraith, "High-fidelity simulations of moving and flexible airfoils at low reynolds numbers," *Experiments in Fluids*, vol. 46, pp. 903–922, 2009.

[10] D. Munday and J. Jacoby, "Active control of separation on a wing with oscillating camber," *AIAA Journal of Aircraft*, vol. 39:1, 2002.

[11] J. D. P. C. B. Lazos, "Flight dynamic simulation assessment of a morphable hyper-ellliptic cambered span winged configuration," in *AIAA Atmospheric Flight Mechanics Conference and Exhibit*, 2003.

[12] M. Abdulrahim, H. Garcia, G. Ivey, and R. Lind, "Flight testing a micro air vehicle using morphing for aeroservoelastic control," in *AIAA/ASME/ASCE/AHS/ASC Structures, Structural Dynamics & Materials Conference*, no. 2004-1674, Reston, VA, 2004, pp. 1776–1792.

[13] B. Stanford, M. A. R. Lind, and P. Ifju, "Investigation of membrane actuation for roll control of a micro air vehicle." *Journal of Aircraft*, vol. 44, pp. 741–741, 2007.

[14] S. Swartz, J. Diaz, D. Riskin, A.S., X.T., D. Willis, and K. Breuer, "Wing structure and the aerodynamic basis of flight in bats," in *45th AIAA Aerospace Sciences Meeting*, vol. 1, 2007, pp. 372–381.

[15] S. Swartz, "Allometric patterning in the limb skeleton of bats: Implications for the mechanics and energetics of powered flight," *Journal of Morphology*, vol. 234, pp. 277–294, 1997.

[16] S. Swartz, M. Groves, H. Kim, and W. Walsh, "Mechanical properties of bat wing membrane skin," *Journal of Zoology*, vol. 239, pp. 357–378, 1996.

[17] R. Wlezien, G. Horner, R. A. McGowan, S. Padula, S. Michael, R. Silcox, and J. Simpson, "Aircraft morphing program," in *Smart Structures and Materials 1998: Industrial and Commercial Applications of Smart Structures Technologies*, J. Sater, Ed., vol. 3326, 1998, pp. 176–187.

[18] K. Lu and S. Kota, "Compliant mechanism synthesis for shape-change applications: Preliminary results," in *Proceedings of SPIE*, V. Rao, Ed., vol. 4693, 2002, pp. 161–172.

[19] J. Bae, N. Kyong, M. Seigler, and D. Inman, "Aeroelastic considerations on shape control of an adaptive wing," *Journal of intelligent material systems and structures*, vol. 16, no. 11-12, pp. 1051–1056, 2005.

[20] B. Dickinson, J. Singler, and B. A. Batten, "Modeling of bioinspired sensors for flow separation detection in micro air vehicles," *Proceedings of the 3rd AIAA Flow Control Conference*, no. AIAA paper 2006-3019, 2006.

[21] ——, "The detection of unsteady flow separation with bioinspired hair cell sensors," *26th AIAA Aerodynamic Measurement Technology and Ground Testing Conference*, no. Paper AIAA-2008-3937, 2008.

[22] B. Dickinson, "Hair receptor sensitivity to changes in laminar boundary layer shape," *Bioinspiration & Biomimetics*, vol. 5, p. 11, 2010.

[23] S. Swartz, "Skin and bones: The mechanical properties of bat wing tissues," *Bats: Phylogeny, Morphology, Echolocation, and Conservation Biology*, pp. 109–126, 1998.

[24] A. Ugural, *Stresses in Plates and Shells*, 2nd ed. McGraw -Hill, 1999.

[25] H. Banks, K. Ito, and B. King, "Theoretical and computational aspects of feedback in structural systems with piezoceramic controllers," in *Computation and Control III*, K. Bowers and J. Lund, Eds., Progress in Systems and Control theory. Birkhauser, 1992.

[26] M. Gockenbach, *Understanding and Implementing the Finite Element Method*. Society for Industrial and Applied Mathematics (SIAM), 2006.

[27] E. Ruggiero, "Modeling and control of spider satellite components," Ph.D. dissertation, Virginia Polytechnic Institute and State University, 2005.

[28] J. Burns and B. King, "Optimal sensor location for robust control of distributed parameter systems," *Proceedings of the 33rd Conference on Decision and Control*, pp. 3967 – 3972, 1994.

[29] A. Faulds and B. King, "Sensor location in feedback control of partial differential equation systems," *Proceedings of the 2000 IEEE International Conference on Control Applications*, pp. 536 – 541, 2000.

[30] H. Banks, R. Smith, and Y. Wang, *Smart Material Structures: Modeling, Estimation and Control*, P. Ciarlet and J.-L. Lions, Eds. John Wiley & Sons, 1996.